

Transport coefficients of hadronic matter in a van der Waals hadron resonance gas model

Ranjita K. Mohapatra¹, Hiranmaya Mishra², Sadhana Dash¹ and Basanta K. Nandi¹

¹*Department of Physics, Indian Institute of Technology Bombay, Mumbai 400076, India*

²*Theory Division, Physical Research Laboratory, Navrangpura, Ahmedabad 380009, India*

We estimate the transport coefficients like shear and bulk viscosities of hot hadronic matter in van der Waals hadron resonance gas (VDW HRG) model in the relaxation time approximation. We also have compared these results with excluded volume hadron resonance (EV HRG) calculations. η/s decreases as the temperature of the hadronic system increases at a fixed baryon chemical potential. η/s in VDW HRG is always less than that of EV HRG case due to the large entropy density in VDW HRG compared to EV HRG case. At a fixed chemical potential, ζ/s in VDW HRG is also less than that of EV HRG case. We also have estimated these transport coefficients along the freezeout curve. There is an increase in chemical freezeout temperature in VDW HRG case determined from the universal condition $E/N = \epsilon/n \sim 1 \text{ GeV}$. We also have calculated the variation of attraction parameter along the freezeout curve $E/N = \epsilon/n \sim 1 \text{ GeV}$ keeping the freezeout parameters same as in ideal HRG and the repulsion parameter fixed. We observe a nontrivial variation of attraction parameter along the freezeout curve where it increases in the meson dominated region and decreases in the baryon dominated region along the chemical freezeout curve. η/s in EV HRG is always large than that VDW HRG along the freezeout curve. This is also true for ζ/s .

I. INTRODUCTION

The large value of elliptic flow observed at Relativistic Heavy Ion Collider (RHIC) and Large Hadron Collider (LHC) confirms that there is a strongly interacting quark gluon plasma (sQGP) produced at these collision energies [1, 2]. The "almost perfect fluid" nature of QGP is produced at RHIC energies with shear viscosity to entropy density ratio i.e $\eta/s \leq 0.2$. This value is close to anti-de Sitter/conformal field theory (AdS/CFT) lower bound on η/s famously known as KSS (Kovtun-Son-Starinets) bound i.e $\eta/s \geq 1/4\pi$ [3]. According to the AdS/CFT, for any strongly interacting fluid η/s has a lower bound i.e $\eta/s \geq 1/4\pi$. This bound has been verified for different fluids like H_2O , N_2 and He_2 etc [4]. The bulk viscosity ζ is zero for any fluid which has conformal symmetry. However, QCD does not have the conformal symmetry around the critical temperature because the trace anomaly $(\epsilon - 3P)/T^4$ shows a peak as observed in the lattice simulations [5, 6]. Perturbative QCD calculations have shown a much higher value of the shear viscosity to the entropy density ratio i.e $\eta/s \geq 1$ [7]. It has been observed that the bulk viscosity is 1000 times smaller than the shear viscosity in the perturbative QCD [7]. But, the non-perturbative nature of QCD is relevant around the phase transition or the crossover region which shows the bulk viscosity is not very small compared to the shear viscosity. The shear viscosity of QGP decreases due to nonzero bulk viscosity coefficient. The nonzero value of the bulk viscosity with nonzero shear viscosity explains the experimental data on the multiplicity, the average transverse momentum and the elliptic flow coefficients very well [8].

The transport coefficients like the shear and the bulk viscosities govern the non-equilibrium system towards the equilibrium state. The shear viscosity shows the resistance to any deformation in the system due to the shear stress and the bulk viscosity shows the resistance to change in the volume of the system. It has been observed that the ratio of shear viscosity to entropy density shows a minimum around the phase transition region [9] and the ratio of bulk viscosity to entropy density shows a maximum around this region [10, 11]. So, these transport coefficients are very important to study the phase transition region and also the QCD critical point.

The transport coefficients like the shear and the bulk viscosities of the QGP phase and the hadronic matter have been calculated by various methods. In principle, the transport coefficients can be calculated directly from QCD using Kubo formulas [12, 13]. However, these calculations are very difficult due to strongly interacting QCD in the region of interest to us. The transport coefficients also have been calculated using Boltzmann equation in the relaxation time approximation [14, 15]. In this relaxation time approximation, the collision integral in Boltzmann equation has been approximated in such a way that the distribution function reaches to the equilibrium distribution function

exponentially with a relaxation time τ . These transport coefficients also have been calculated in Chapman-Enskog method [13, 16]. These also have been calculated using effective field theory models and quasiparticle model [17–19]. These are also other kinetic theory calculations on transport coefficients [20–25] etc.

In this work, we would like to estimate the shear and the bulk viscosity of the hot hadronic matter in a van der Waals hadron resonance gas (VDW HRG) using the relaxation time approximation. The ratio of shear viscosity to entropy density of hadronic matter also has been shown in VDW HRG with different attraction and repulsion parameters than described here in ref[26]. The ideal HRG (IHRG) model which describes the hadrons as point particles successfully explains the lattice data for different thermodynamic quantities at low temperature. But, there is a mismatch between the lattice results and IHRG calculations around the critical temperature [27, 28]. This mismatch has been taken care of upto some level by taking finite radius of hadrons in the excluded volume (EV HRG) procedure in a grand canonical ensemble [29]. There is repulsive interaction between hadrons due to finite radius (hard core repulsion) in EV HRG model. However, apart from hard core repulsion, there is van der Waals attraction between the hadrons (VDW HRG model). The calculations of the thermodynamic quantities in VDW HRG model matches well with the lattice results around the critical temperature [30–33].

This paper is organized as follows. we discuss the essential aspects of the HRG model in section II. Section III describes the estimation of the transport coefficients like shear and bulk viscosities in the relaxation time approximation. Section IV describes the results obtained in VDW HRG model. Then we conclude in Section V.

II. HADRON RESONANCE GAS MODEL

A. Ideal and excluded volume model

The IHRG model successfully describes the thermodynamic quantities and matches with the lattice QCD calculations. The hadrons are treated as point particles in the model and the thermodynamic quantities blows up as the system approaches the critical temperature. However, the hadrons are not point particles, there is repulsive interaction between these hadrons due to their finite size and this has been taken in EV HRG model.

The grand canonical partition function of IHRG for each hadron species is written as

$$\ln Z_i^{id} = \pm V g_i \int \frac{d^3p}{(2\pi)^3} \ln \left[1 \pm e^{-(E_i - \mu_i)/T} \right] \quad (1)$$

Here \pm corresponds to fermions and bosons respectively. Here V is the volume of the system, g_i is the spin degeneracy factor, $E_i = \sqrt{p^2 + m_i^2}$ is the single particle energy and $\mu_i = B_i \mu_B + S_i \mu_S + Q_i \mu_Q$ is the chemical potential. Here B_i , S_i and Q_i are the baryon number, strange and electric charge of the particle and μ_B , μ_S and μ_Q are the corresponding chemical potentials. All the thermodynamic quantities like pressure, energy density and entropy density etc. can be derived from this partition function.

In a thermodynamically consistent EV HRG model, the pressure is given by

$$P^{EV}(T, \mu) = \sum_i p_i^{id}(T, \mu^*) \quad (2)$$

where the chemical potential for i th hadron is given by

$$\mu^* = \mu - V_{ex} P^{EV} \quad (3)$$

where $V_{ex} = 16\pi r^3/3$ the excluded volume for each hadron with hard core radius r . The number density, entropy density and energy density in EV HRG is given by

$$n^{EV}(T, \mu) = \frac{\sum_i n_i^{id}(T, \mu_i^*)}{1 + V_{ex} \sum_i n_i^{id}(T, \mu_i^*)} \quad (4)$$

$$s^{EV}(T, \mu) = \frac{\sum_i s_i^{id}(T, \mu_i^*)}{1 + V_{ex} \sum_i s_i^{id}(T, \mu_i^*)} \quad (5)$$

$$\epsilon^{EV}(T, \mu) = \frac{\sum_i \epsilon_i^{id}(T, \mu_i^*)}{1 + V_{ex} \sum_i \epsilon_i^{id}(T, \mu_i^*)} \quad (6)$$

$$(7)$$

B. van der Walls hadron resonance gas

The grand canonical ensemble formulation of the full VDW equation with both attractive and repulsive interactions, was developed in [30–33]. The attractive parameter a and the repulsive parameter b of VDW HRG are uniquely fixed by reproducing the nuclear saturation density $n_0 = 0.16 \text{ fm}^{-3}$ and binding energy $E/A = -16 \text{ MeV}$ of the ground state of nuclear matter. For nucleons the values $a = 329 \text{ MeV fm}^3$ and $b = 3.42 \text{ fm}^3$ were obtained. This value of b corresponds to a nucleon radius $\sim 0.58 \text{ fm}$ from the relation $b = 16\pi r^3/3$. This model predicts a liquid-gas first order phase transition in nuclear matter with a critical point at $T_c \simeq 19.7 \text{ MeV}$ and $\mu_c \simeq 908 \text{ MeV}$.

However, the VDW interactions have been taken between baryons-baryons and antibaryons-antibaryons in VDW HRG model [33]. The VDW parameters a and b for all (anti)baryons are assumed to be equal to those of nucleons. The baryon-antibaryon, meson-meson, and meson- (anti)baryon VDW interactions are neglected. The baryon-antibaryon VDW interactions are neglected because short-range interactions between baryons and antibaryons may be dominated by annihilation processes [33]. The meson-meson VDW interactions also have been neglected because of the significant mesonic eigen volume, comparable to those of baryons, leads to significant suppression of thermodynamic functions in the crossover region at $\mu_B = 0$ which does not match with lattice data [33]. The attractive interactions between mesons lead to resonance formation, which have been already included in the HRG model.

The VDW HRG model consists of three subsystem: Noninteracting mesons, VDW baryons, and VDW antibaryons. The total pressure is given by

$$P(T, \mu) = P_M(T, \mu) + P_B(T, \mu) + P_{\bar{B}}(T, \mu). \quad (8)$$

where

$$P_M(T, \mu) = \sum_{i \in M} p_i^{\text{id}}(T, \mu_i). \quad (9)$$

$$P_B(T, \mu) = \sum_{i \in B} p_i^{\text{id}}(T, \mu_i^{B*}) - a n_B^2. \quad (10)$$

$$P_{\bar{B}}(T, \mu) = \sum_{i \in \bar{B}} p_i^{\text{id}}(T, \mu_i^{\bar{B}*}) - a n_{\bar{B}}^2. \quad (11)$$

Here M stands for mesons, B for baryons, and \bar{B} for antibaryons, p_i^{id} is the Fermi or Bose ideal gas pressure, $\mu_i^{B(\bar{B})*} = \mu_i - b P_{B(\bar{B})} - a b n_{B(\bar{B})}^2 + 2 a n_{B(\bar{B})}$, and n_B and $n_{\bar{B}}$ are total densities of baryons and antibaryons respectively.

The number density, entropy density and energy density for baryons and antibaryons in VDW HRG are given by:

$$n_{B(\bar{B})} = \frac{\sum_{i \in B(\bar{B})} n_i^{\text{id}}(T, \mu_i^{B(\bar{B})*})}{1 + b \sum_{i \in B(\bar{B})} n_i^{\text{id}}(T, \mu_i^{B(\bar{B})*})}. \quad (12)$$

$$s_{B(\bar{B})} = \frac{\sum_{i \in B(\bar{B})} s_i^{\text{id}}(T, \mu_i^{B(\bar{B})*})}{1 + b \sum_{i \in B(\bar{B})} n_i^{\text{id}}(T, \mu_i^{B(\bar{B})*})}. \quad (13)$$

$$\epsilon_{B(\bar{B})} = \frac{\sum_{i \in B(\bar{B})} \epsilon_i^{\text{id}}(T, \mu_i^{B(\bar{B})*})}{1 + b \sum_{i \in B(\bar{B})} n_i^{\text{id}}(T, \mu_i^{B(\bar{B})*})} - a n_{B(\bar{B})}^2(T, \mu). \quad (14)$$

$$(15)$$

The thermodynamic quantities in VDW HRG model obey the self consistency relation $Ts = \epsilon + P - \mu n$. We have incorporated all the hadrons listed in the particle data book upto mass 3 GeV [34].

III. TRANSPORT COEFFICIENTS IN RELAXATION TIME APPROXIMATION

Here we briefly describe the estimation of transport coefficients like shear and bulk viscosity in the relaxation time approximation [14].

The Boltzmann transport equation of kinetic theory is given by

$$\frac{\partial f_p}{\partial t} + v_p^i \frac{\partial f_p}{\partial x^i} = C[f_p]. \quad (16)$$

where f_p is the single particle distribution function, $\vec{v}_p = \vec{p}/E_p$ is particle velocity and $C[f_p]$ is the collision integral. The collision integral gives the rate of change of the distribution function due to collisions of the constituent particles of the system. However, this is a very complicated integral to solve. So, this collision integral has been approximated such that the non-equilibrium distribution function f_p approaches to the equilibrium distribution f_p^0 exponentially with a relaxation time τ which is of the order of collision time. Hence, the collision integral in the relaxation time approximation is given by

$$C[f_p] \simeq -\frac{(f_p - f_p^0)}{\tau(E_p)} = -\frac{\delta f_p}{\tau} \quad (17)$$

The relaxation time τ depends on the energy of the particle. The equilibrium distribution function f_p^0 is given by

$$f_p^0 = \frac{1}{\exp\left(\frac{E_p - \vec{p} \cdot \vec{u} - \mu}{T}\right) \pm 1} \quad (18)$$

Here \vec{u} is the fluid velocity and \pm corresponds to fermions and bosons respectively. In hydrodynamics, the stress energy tensor is defined as

$$T^{\mu\nu} = T_0^{\mu\nu} + T_{dissi}^{\mu\nu} \quad (19)$$

where $T_0^{\mu\nu}$ is the ideal part of the fluid when there is no dissipation of the fluid taken into account. $T_{dissi}^{\mu\nu}$ is the dissipative part of the fluid from where shear and bulk viscosities can be calculated.

The shear and the bulk viscosities are related to the dissipative part of stress energy tensor

$$T_{dissi}^{ij} = -\eta \left(\frac{\partial u^i}{\partial x^j} + \frac{\partial u^j}{\partial x^i} \right) - \left(\zeta - \frac{2}{3}\eta \right) \frac{\partial u^i}{\partial x^j} \delta^{ij} \quad (20)$$

The stress energy tensor in terms of the distribution function given by

$$T^{\mu\nu} = g \int \frac{d^3 p}{(2\pi)^3 p_0} p^\mu p^\nu f_p \quad (21)$$

Here g is the degeneracy of the particle. Also

$$f_p = f_p^0 + \delta f_p \quad (22)$$

So using Eq. (21) and Eq. (22), the dissipative part of stress energy tensor given by

$$T_{dissi}^{ij} = g \int \frac{d^3 p}{(2\pi)^3 p_0} p^i p^j \delta f_p \quad (23)$$

From Eqs. (16) and (17)

$$\delta f_p = -\tau(E_p) \left(\frac{\partial f_p^0}{\partial t} + v_p^i \frac{\partial f_p^0}{\partial x^i} \right) \quad (24)$$

For one dimensional flow of the form $u^i = (u_x(y), 0, 0)$, Eq. (20) simplifies to

$$T_{dissi}^{xy} = -\eta \partial u_x / \partial y. \quad (25)$$

Using Eqs. (23), (24) and (18), one can obtain

$$T_{dissi}^{xy} = \left\{ -\frac{g}{T} \int \frac{d^3p}{(2\pi)^3} \tau(E_p) \left(\frac{p_x p_y}{E_p} \right)^2 f_p^0 \right\} \frac{\partial u_x}{\partial y} \quad (26)$$

Equating Eq. (25) and Eq. (26), we obtain the expression for shear viscosity

$$\eta = \frac{g}{15T} \int \frac{d^3p}{(2\pi)^3} \tau(E_p) \frac{p^4}{E_p^2} f_p^0 \quad (27)$$

Taking the trace of Eq. (20), we obtain bulk viscosity

$$(T_{dissi})_i^i = -3\zeta \frac{\partial u^i}{\partial x^i} \quad (28)$$

From Eq. (23), we also get

$$(T_{dissi})_i^i = -g \int \frac{d^3p}{(2\pi)^3} \tau(E_p) \frac{p^2}{E_p} \left(\frac{\partial f_p^0}{\partial t} + v_p^i \frac{\partial f_p^0}{\partial x^i} \right) \quad (29)$$

From Eqs. (28) and (29), and using the energy momentum conservation equation $\partial_\mu T^{\mu\nu} = 0$, one can obtain

$$\zeta = \frac{g}{T} \int \frac{d^3p}{(2\pi)^3} \tau(E_p) f_p^0 \left[E_p C_{n_B}^2 \pm \left(\frac{\partial P}{\partial n_B} \right)_\epsilon - \frac{p^2}{3E_p} \right]^2 \quad (30)$$

Here \pm corresponds to particles and anti particle respectively. $C_{n_B}^2 = \frac{\partial P}{\partial \epsilon}|_{n_B}$, is the speed of sound at constant baryon density.

For a hadron resonance gas, the shear and bulk viscosities can be written as a sum over all the particles included in this model

$$\eta = \frac{1}{15T} \sum_a \int \frac{g_a d^3p}{(2\pi)^3} \frac{p^4}{E_a^2} (\tau_a f_a^0) \quad (31)$$

$$\zeta = \frac{1}{T} \sum_a \int \frac{g_a d^3p}{(2\pi)^3} \left\{ \tau_a f_a^0 \left[E_a C_{n_B}^2 \pm \left(\frac{\partial P}{\partial n_B} \right)_\epsilon - \frac{p^2}{3E_a} \right]^2 \right. \quad (32)$$

Here a corresponds to all the hadrons taken in VDW HRG model.

The average relaxation time for a hadron a is given by

$$\tilde{\tau}_a^{-1} = \sum_b n_b \langle \sigma_{ab} v_{ab} \rangle \quad (33)$$

here the summation is over all other hadrons in VDW HRG model. n_b is the number density of the hadron b .

For any scattering process $a(p_a) + b(p_b) \rightarrow a(p_c) + b(p_d)$, the thermal averaged cross section times the relative velocity is given by

$$\langle \sigma_{ab} v_{ab} \rangle = \frac{\sigma}{8T m_a^2 m_b^2 K_2\left(\frac{m_a}{T}\right) K_2\left(\frac{m_b}{T}\right)} \int_{(m_a+m_b)^2}^{\infty} dS \frac{[S - (m_a - m_b)^2]}{\sqrt{S}} [S - (m_a + m_b)^2] K_1(\sqrt{S}/T) \quad (34)$$

Here K_n is the modified Bessel function of order n . The cross section σ in Eq. (34) in terms of hadron radius r is given by $\sigma = 4\pi r^2$.

IV. RESULTS AND DISCUSSION

In order to calculate the shear and the bulk viscosity of the hot hadronic matter, one needs an estimation of the average relaxation time τ with respect to the temperature of the system. Here the average is taken over all the hadrons with same radius ~ 0.5 fm. Fig.1 shows the variation of the relaxation time with respect to the temperature at three different chemical potentials. At a fixed chemical potential, the relaxation time decreases as the temperature increases. This is due to the fact that the number density increases as the temperature increases and τ is inversely proportional to the number density according to Eq. (33). The average relaxation time also decreases as the chemical potential increases at a fixed temperature. This is because the baryon number density increases as the chemical potential increases. At $\mu_B = 0$, the average relaxation time decreases from ~ 10 fm to ~ 0.2 fm as the temperature of the hadronic system increases from 100 MeV to 200 MeV.

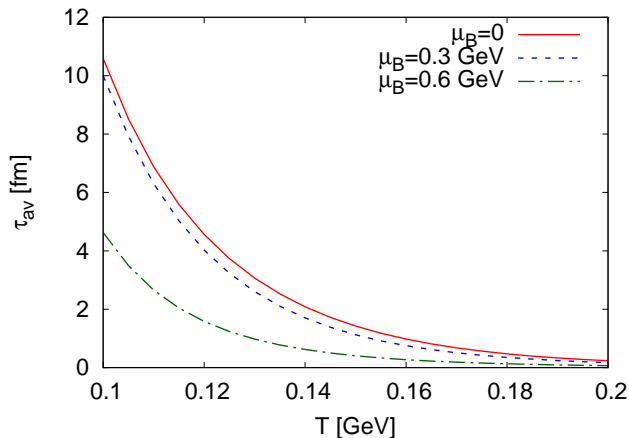


FIG. 1:

The average relaxation time with respect to temperature at three different baryon chemical potentials.

The normalized entropy density for VDW HRG model is given for different conditions in Fig.2 at different chemical potentials. At $\mu_B = 0$, the solid curve shows the variation of normalized entropy density for an ideal HRG model. The dotted curve represents the normalized entropy density when the attraction parameter a of VDW HRG model is zero, but the repulsion parameter $b = 3.42$ fm³ as in VDW HRG model. This is equivalent to the EV HRG model where there is only hard core repulsion between the hadrons. However, here the repulsion has been taken only between baryon-baryon and antibaryon-antibaryon (as in VDW HRG model). Due to only the hard core repulsion i.e $a = 0$, the normalized entropy density decreases compared to the ideal HRG. This is prominent after a temperature 160 MeV at $\mu_B = 0$. When the repulsion parameter b of VDW HRG is zero (equivalent to point particles as in the ideal HRG), but the attraction term is $a = 329$ MeV fm³ as in VDW HRG, the entropy density increases compared to the ideal HRG due to the attraction term. When both the parameters (attraction and repulsion) are non zero as in VDW HRG, the normalized entropy density falls in between the ideal HRG and the EV HRG (i.e $a = 0$). This trend is also true for higher chemical potentials as shown in Fig.2b and Fig.2c. The normalized entropy density is always large for the large chemical potentials. One can see from Fig.2, the splitting between different curves occurs at the lower temperature for higher chemical potential. As one can see from Fig.2a, the splitting between different curves occurs at a temperature ~ 160 MeV at $\mu_B = 0$. This splitting occurs at a lower temperature ~ 130 MeV at $\mu_B = 0.3$ GeV (Fig.2b) and at ~ 100 MeV at $\mu_B = 0.6$ GeV (Fig.2c). This is because when the baryon chemical potential is large, there are more baryons in the system compared to mesons. Since the VDW interactions have been taken among baryons-baryons and antibaryons-antibaryons, the VDW parameters play a significant role at a lower temperature for higher chemical potentials.

Fig.3 shows the variation of η with respect to the temperature at three different chemical potentials. η increases monotonically with the temperature at any fixed chemical potential. This is because the number density increases as the temperature increases. η also increases as the chemical potential increases at a fixed temperature. This is due to the fact that the number density of baryons increases at higher chemical potential.

It is very important to measure the dimensionless quantity η/s rather than η . η/s has been shown for two different cases (i.e $a = 0$ and VDW HRG) at different chemical potentials in Fig.4. Fig.4a shows the variation of η/s with respect to the temperature at $\mu_B = 0$ for these two different cases. We can see the different curves almost overlap with each other at $\mu_B = 0$. This is because the entropy density is almost the same for these two cases up to temperature

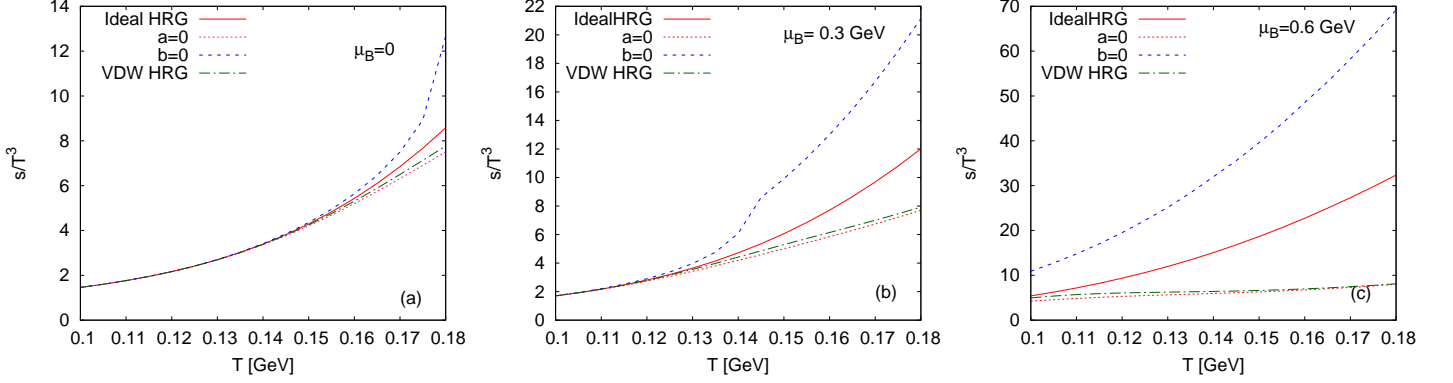


FIG. 2:

The normalized entropy density curve at (a) $\mu_B = 0$, (b) $\mu_B = 0.3 \text{ GeV}$ and (c) $\mu_B = 0.6 \text{ GeV}$.

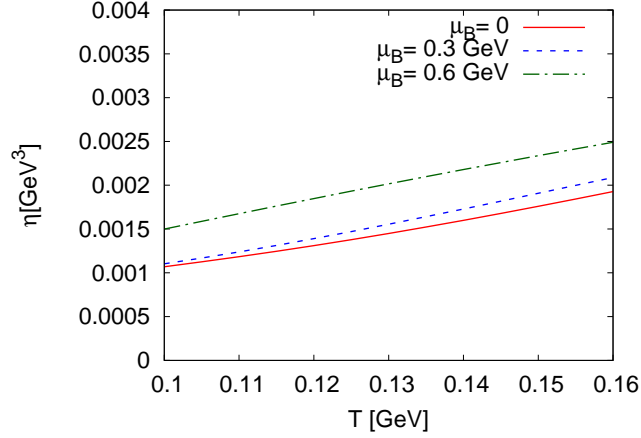


FIG. 3:

Plot of η with respect to temperature at different baryon chemical potentials.

160 MeV as shown in Fig.2a. η is also the same for these two different cases since each hadron has the same radius. η/s approaches to the famous KSS bound at temperature 160 MeV for the hot hadronic matter at $\mu_B = 0$. This is very close to the critical temperature $\sim 170 \text{ MeV}$ at $\mu_B = 0$ where an almost perfect fluid nature of QGP has been observed. Fig.4b shows the variation of η/s with respect to the temperature at $\mu_B = 300 \text{ MeV}$. η/s is almost the same for VDW HRG model and $a = 0$ case due to the reasons explained above. This is also true for $\mu_B = 600 \text{ MeV}$ as shown in Fig.4c. However at higher $\mu_B = 600 \text{ MeV}$, η/s is different for the two different cases at lower temperature. This is due to the small difference in the entropy density at lower temperature as shown in Fig.2c. One can clearly see η/s approaches the KSS bound at a relatively higher temperature for higher chemical potential. We also can see η/s decreases as chemical potential increases at a fixed temperature. This is because the entropy density is large for higher chemical potential.

Fig.5 shows the variation of ζ with respect to temperature at two different chemical potentials $\mu_B = 0$ and $\mu_B = 600 \text{ MeV}$. One can see ζ at $\mu_B = 0$ is same for both EV HRG and VDW HRG case. This is mainly because the repulsion parameter is same for both the case and the attraction parameter in VDW HRG does not affect ζ at $\mu_B = 0$ due to equal number of baryons and antibaryons. When μ_B increases, ζ increases. The shear viscosity is larger for VDW HRG compared to EV HRG at $\mu_B = 600 \text{ MeV}$. This is because there are more baryons compared to antibaryons in the system at $\mu_B = 600 \text{ MeV}$ and the attraction parameter is considered in between baryons- baryons and antibaryons-antibaryons.

Fig.5 shows the variation of ζ/s with respect to temperature at two different chemical potentials $\mu_B = 0$ and $\mu_B = 600 \text{ MeV}$. ζ/s is less in VDW HRG compared to EV HRG at $\mu_B = 0$ due to the fact that the entropy density in VDW HRG is large compared to EV HRG. This is also true at $\mu_B = 600 \text{ MeV}$. The nontrivial variation of ζ/s

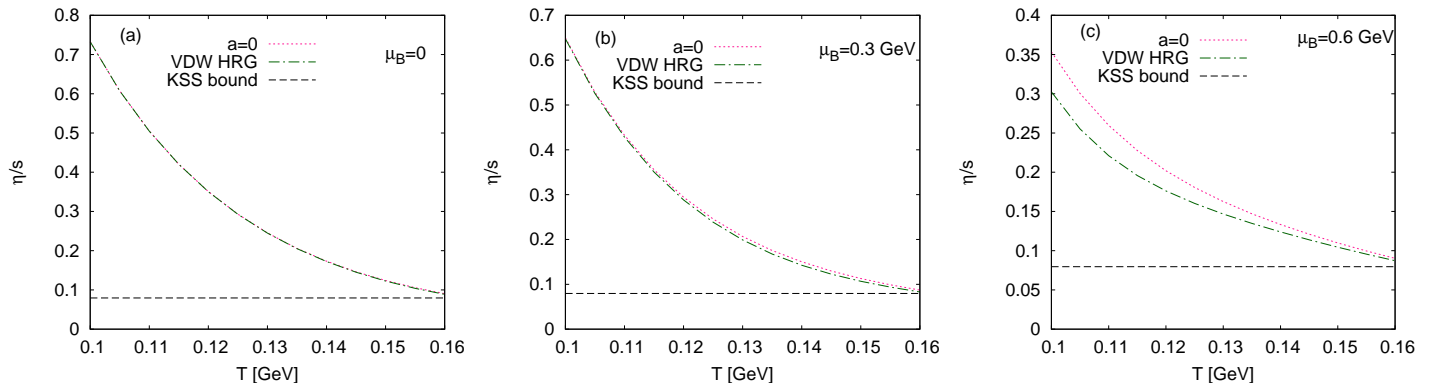


FIG. 4:

Plot of η/s with respect to temperature at (a) $\mu_B = 0$, (b) $\mu_B = 0.3 \text{ GeV}$ and (c) $\mu_B = 0.6 \text{ GeV}$.

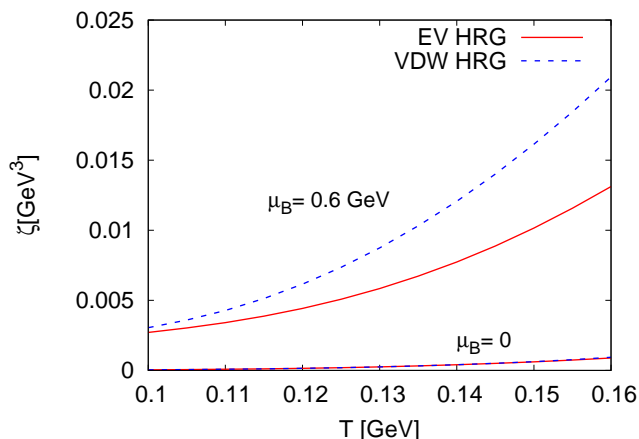


FIG. 5:

Plot of ζ with respect to temperature at $\mu_B = 0$ and $\mu_B = 0.6 \text{ GeV}$.

with temperature in VDW HRG at $\mu_B = 600 \text{ MeV}$ is due to the nontrivial variation of entropy density.

Now we estimate the transport coefficients of the hadronic matter along the chemical freezeout curve. First we will discuss the effect of VDW attraction and repulsion terms on the universal chemical freezeout curve determined by the condition $E/N = \epsilon/n \sim 1 \text{ GeV}$ [35]. This is shown in Fig.7. Since ϵ and n are extensive quantities, their ratio is almost independent of the volume. Hence, the chemical freezeout parameters remain unchanged in the EV HRG model [36]. However, the chemical freezeout temperature in VDW HRG is larger than that ideal HRG as shown in Fig.7. The energy density expression i.e Eq. (15) in VDW HRG has two terms. The first term expresses the decrease in energy density due to the repulsion parameter b as in the EV HRG model. But the second term (with the attraction parameter) with a negative sign further decreases the energy density in VDW HRG model. The number density (Eq. (28)) in VDW HRG mainly decreases due to the repulsion term. So, the energy density decreases faster than the number density in VDW HRG model. So to keep the ratio $\epsilon/n \sim 1 \text{ GeV}$ fixed, the temperature has to be increased in VDW HRG compared to the ideal HRG calculations. This VDW HRG model with shifted chemical freezeout temperature, the attraction and repulsion parameters are $a = 329 \text{ MeV fm}^3$ and $b = 3.42 \text{ fm}^3$ respectively along the freezeout line, is described as VDW HRG 1 model. It has been shown that there is a shift (decrease) in the chemical freezeout temperature at non zero magnetic field due to inverse magnetic catalysis effect in the HRG model [37, 38]. Here we show that there is shift (increase) in the chemical freezeout temperature due to VDW interactions at zero magnetic field.

We have taken fixed values of attraction and repulsion parameters i.e $a = 329 \text{ MeV fm}^3$ and $b = 3.42 \text{ fm}^3$ at all temperatures and chemical potentials in all VDW HRG calculations above. However, it has been already shown that these parameters can vary [26]. In this work [26], the authors have taken different values of $a = 926 \text{ MeV fm}^3$ and $b = 4.08 \text{ fm}^3$ to match lattice results for $\mu_B/T = 1$ and $\mu_B/T = 2$. Here this value of b corresponds to a larger radius

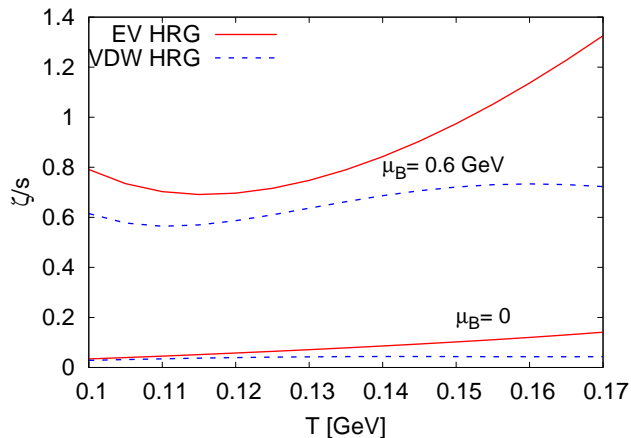


FIG. 6:

Plot of ζ/s with respect to temperature at (a) $\mu_B = 0$ and $\mu_B = 0.6$ GeV.

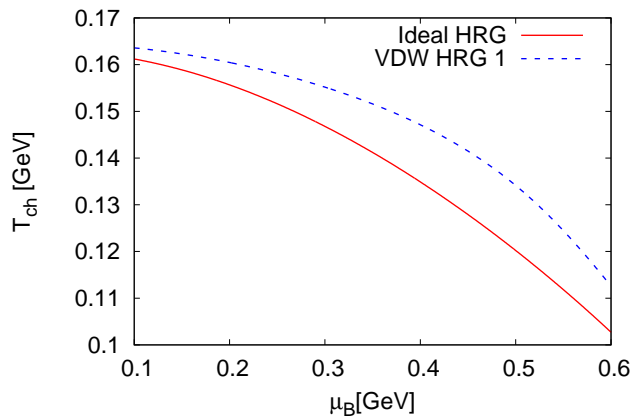


FIG. 7:

The universal chemical freezeout curve determined by $\epsilon/n \sim 1$ GeV.

i.e ~ 0.62 fm. There is no first principle calculation for these parameters. Since the repulsion parameter b depends on the radius r of hadron i.e $b = 16\pi r^3/3$, we simply can take this to be a fixed parameter i.e $b = 3.42$ fm³. Once b is fixed and the chemical freezeout temperature and baryon chemical potential are fixed as for ideal HRG calculations (since these values match with experimental value of freezeout parameters) corresponding to the solid curve in Fig.7. The universal chemical freezeout curve determined by the condition $\epsilon/n \sim 1$ GeV fixes the attraction parameter a as shown in Fig.8. This VDW HRG model with the chemical freezeout parameters same as the ideal HRG, the repulsion parameter $b = 3.42$ fm³ and the attraction parameter a varying along the freezeout line is described as VDW HRG 2 model. we can see that attraction parameter a increases along the freezeout curve upto $\mu_B \simeq 300$ MeV and decreases after that. This is because the system is meson dominated upto this chemical potential and after this it is baryon dominated [39]. Since VDW interactions have been taken between baryons-baryons, antibaryons-antibaryons and switched off between mesons in VDW HRG 2, the attraction parameter has to increase with chemical potential initially in the meson dominated region and to decrease with chemical potential in the baryon dominated region to keep the ratio $\epsilon/n \sim 1$ GeV fixed. We also have shown the variation of attraction parameter a along the freezeout curve for $b = 4.08$ fm³ in Fig.8. The energy density and the number density decrease faster corresponding to the large radius of hadron for $b = 4.08$ fm³. So to keep the ratio $\epsilon/n \sim 1$ GeV fixed at a particular freezeout temperature and chemical potential, the attraction parameter has to be increased for $b = 4.08$ fm³ compared to $b = 3.42$ fm³ as shown in Fig.8. It goes from a meson dominated region to a baryon dominated region at a lower chemical potential for higher b as shown in Fig.8.

We have shown the variation of η/s along the freezeout curve for three different cases in Fig.9. The dotted line shows

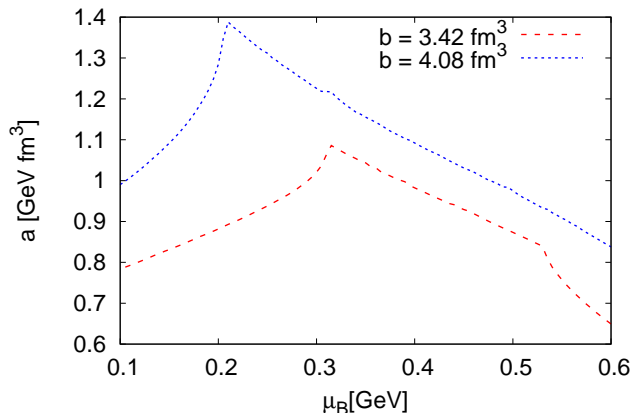


FIG. 8:

Variation of attraction parameter a along the chemical freezeout curve determined by $\epsilon/n \sim 1 \text{ GeV}$.

η/s for EV HRG case where we have taken each hadron (all baryons and mesons) has a radius 0.58 fm corresponding to $b = 3.42 \text{ fm}^3$. This is along the freezeout parameters shown by the solid line in Fig.7. since the chemical freezeout parameters in the EV HRG model remain the same as in the ideal HRG. VDW HRG 1 describes η/s along the shifted chemical freezeout parameters shown by the dashed line in Fig.7. The values of the attraction and the repulsion parameters for this VDW HRG 1 are $a = 329 \text{ MeV fm}^3$ and $b = 3.42 \text{ fm}^3$ respectively. Fig.9 shows the variation of η/s in VDW HRG 2 along the chemical freezeout curve shown by the solid line, where the attraction parameter is varying as shown by the dashed curve in Fig.8 and the repulsion parameter $b = 3.42 \text{ fm}^3$ for this case. Here the repulsion parameter in VDW HRG $b = 3.42 \text{ fm}^3$ corresponds to the same radius $\sim 0.58 \text{ fm}$ as in EV HRG. So, η is same for EV HRG and VDW HRG 2 case since the chemical freezeout parameters and the radius of hadrons are same for both the cases. η is relatively large for VDW HRG 1 due to higher freezeout temperature. The entropy density is small in EV HRG model compared to VDW HRG 2 model, since there is only repulsion in EV HRG model compared to attractions and repulsions in VDW HRG 2 model. So, η/s in VDW HRG 2 falls below EV HRG model calculations along the freezeout curve. Again, the entropy density of VDW HRG 1 is large compared to VDW HRG 2 since the freezeout temperature is large in VDW HRG 1 compared to VDW HRG 2. So, η/s in VDW HRG 1 and VDW HRG 2 are almost the same due to the interplay of large freezeout temperature in VDW HRG 1 and large attraction parameter in VDW HRG 2. It has been shown that η/s increases as the chemical potential increases along the freezeout line, this is due to the fact that the freezeout temperature decreases as the chemical potential increases and the entropy density decreases due the decrease in the freezeout temperature. It is in agreement with the fact that at low chemical potentials (higher collision energies) QGP is a perfect fluid and the hot hadronic matter originating from it respects this nature.

We have shown the variation of ζ/s along the freezeout curve for three different cases in Fig.10. ζ/s increases as the chemical potential increases along the freezeout curve due to the decrease in entropy density. ζ/s is large for EV HRG compared to other two cases. The nontrivial dependence of ζ/s along the freezeout curve for VDW HRG 2 is due to the nontrivial dependence of attraction parameter along the freezeout curve. So the nontrivial dependence of attraction parameter along the freezeout curve plays an important role in the calculation of bulk viscosity.

V. CONCLUSIONS

We have estimated the transport coefficients like shear and bulk viscosity of hot hadronic matter in VDW HRG model in a relaxation time approximation and compared these with the estimates obtained in EV HRG model. The average relaxation time has been calculated with respect to the temperature of the system and this relaxation time decreases as temperature increases. It has been shown that the attraction and repulsion parameters of VDW HRG play an important role in the calculation the entropy density at higher μ_B since these VDW interactions has been taken between baryons-baryons and antibaryons-antibaryons. The shear viscosity η increases as the temperature of the system increases and it also increases with the chemical potential. But the important quantity η/s decreases as temperature increases due to the fact that the entropy density increases with respect to temperature. η/s for VDW HRG is far above the KSS bound at lower temperature and it approaches to the lower bound at higher temperature.

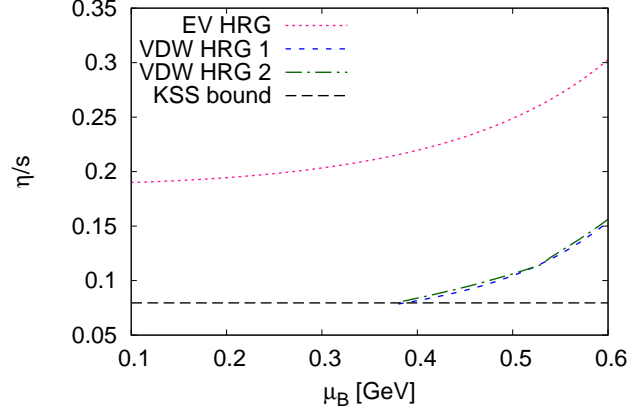


FIG. 9:
Plot of η/s along the chemical freezeout curve.

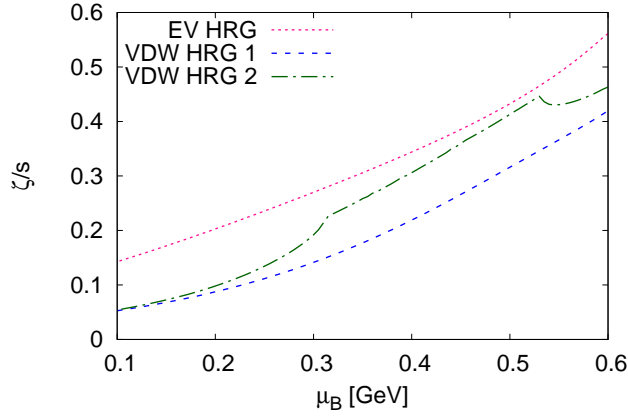


FIG. 10:
Plot of ζ/s along the chemical freezeout curve.

At higher chemical potential, it approaches the KSS bound even at relatively higher temperature. The attraction parameter in VDW HRG plays very important role in the calculation of bulk viscosity at higher chemical potential. The bulk viscosity is same for EV HRG and VDW HRG at $\mu_B = 0$, but at higher chemical potential i.e $\mu_B = 600$ MeV ζ for VDW HRG is large that EV HRG. However, ζ/s is larger for EV HRG compared to VDW HRG due to the decrease in entropy density in EV HRG compared to VDW HRG. The nontrivial dependence of ζ/s with respect to temperature in VDW HRG at $\mu_B = 600$ MeV is due to the nontrivial variation of entropy density with respect to temperature in this model.

It is very important to estimate these transport coefficients along the chemical freezeout curve where this hadronic system is chemically equilibrated. We have shown the chemical freezeout curve determined from the condition $\epsilon/n \sim 1$ GeV for ideal HRG and compared it with VDW HRG case. The chemical freezeout curve for VDW HRG is shifted to higher temperature due to the fast decrease of the energy density compared to the number density in VDW HRG. This chemical freezeout curve with higher freezeout temperature, the attraction and repulsion parameters as constants along the freezeout curve is represented as VDW HRG 1 model. However, one can take the freezeout parameters as in ideal HRG, the repulsion parameters corresponding to the hadron radius as fixed quantities. Then the universal freezeout curve determined from the condition $\epsilon/n \sim 1$ GeV fixes the attraction parameter along the freezeout curve. This freezeout curve is known as VDW HRG 2 model. The attraction parameter in VDW HRG 2 model increases as baryon chemical potential increases upto 300 MeV and then decreases along the freezeout curve. This is due to the fact that the system is meson dominated upto $\mu_B = 300$ MeV and then it is baryon dominated. The VDW

interactions has been taken between baryons-baryons and antibaryons-antibaryons. So the attraction parameter is to be increased in the meson dominated region and to be decreased in the baryon dominated region to keep $\epsilon/n \sim 1$ GeV fixed at those chemical freezeout parameters. We have estimated η/s along the freezeout curve for EV HRG, VDW HRG 1 and VDW HRG 2 case. η/s is larger for EV HRG case compared to other two cases. This is mainly due to the fact that the entropy density is small in EV HRG model due to only repulsion parameter among the hadrons. η/s for VDW HRG 1 and VDW HRG 2 are almost same due to interplay of higher freezeout temperature in VDW HRG 1 and higher attraction parameter in VDW HRG 2. Similarly, ζ/s is larger for EV HRG case compared to other two cases. ζ/s varies nontrivially along the freezeout curve in VDW HRG 2 due to the nontrivial variation of the attraction parameter. So, these transport coefficients in VDW HRG model (with attraction and repulsion among hadrons) are very different than that of EV HRG model (with only repulsion among hadrons).

Acknowledgments

We would like to thank Arpan Das and Guru Prakash Kadam for very useful discussions and suggestions.

-
- [1] P. Romatschke and U. Romatschke, Phys. Rev. Lett. **99**, 172301 (2007).
 - [2] K. Aamodt et al. (ALICE Collaboration), Phys. Rev. Lett. **105**, 252302 (2010).
 - [3] P. Kovtun, D. T. Son, and A. O. Starinets, Phys. Rev. Lett. **94**, 111601 (2005).
 - [4] R. A. Lacey, N. N. Ajitanand, J. M. Alexander, P. Chung, W. G. Holzmann, M. Issah, A. Taranenko, P. Danielewicz, and H. Stcker, Phys. Rev. Lett. **98**, 092301 (2007).
 - [5] A. Bazavov et al., Phys. Rev. **D 90**, 094503 (2014).
 - [6] S. Borsonyi et al., J. High Energy Phys. **11** 077 (2010).
 - [7] P. Arnold, C. Dogan, and G. D. Moore Phys. Rev. **D 74**, 085021 (2006).
 - [8] S. Ryu, J.-F. Paquet, C. Shen, G.S. Denicol, B. Schenke, S. Jeon, and C. Gale Phys. Rev. Lett. **115**, 132301 (2015).
 - [9] L. P. Csernai, J. I. Kapusta, and L. D. McLerran, Phys. Rev. Lett. **97**, 152303 (2006).
 - [10] J. I. Kapusta, in Relativistic Heavy Ion Physics, Landolt- Bornstein Group 1, Vol. 23 (Springer, New York, 2010).
 - [11] D. Kharzeev and K. Tuchin, J. High Energy Phys. **09**,093 (2008).
 - [12] F. Karsch, D. Kharzeev, and K. Tuchin, Phys. Lett. **B 663**, 217 (2008).
 - [13] S. Plumari, A. Paglisi, F. Scardina, V. Greco Phys. Rev. **C 83**, 054902 (2012).
 - [14] S. Gavin, Nucl. Phys. **A 435**, 826 (1985).
 - [15] G. P. Kadam and H. Mishra, Phys. Rev. **C 92**, 035203 (2015).
 - [16] S. R. de Groot, W. A. van Leeuwen, and C. Weert, Relativistic Kinetic Theory, Principles and Applications (North-Holland, Amsterdam, 1980).
 - [17] R. Marty, E. Bratkovskaya, W. Cassing, J. Aichelin, and H. Berrehrh Phys. Rev. **C 88**, 045204 (2013).
 - [18] A. Abhishek, H. Mishra, and S. Ghosh Phys. Rev. **D 97**, 014005 (2018).
 - [19] P. Chakraborty and J. I. Kapusta, Phys. Rev. **C 83**, 014906 (2011).
 - [20] N. Demir and S. A. Bass, Phys. Rev. Lett. **102**, 172302 (2009).
 - [21] A. Muronga, Phys. Rev. **C 69**, 044901 (2004).
 - [22] A. Dobado and F. J. Llanes-Estrada, Phys. Rev. **D 69**, 116004 (2004).
 - [23] J.W. Chen, Y. H. Li, Y. F. Liu, and E. Nakano, Phys. Rev. **D 76**, 114011 (2007).
 - [24] K. Itakura, O. Morimatsu, and H. Otomo, Phys. Rev. **D 77**, 014014 (2008).
 - [25] C. Sasaki and K. Redlich, Phys. Rev. **C 79**, 055207 (2009).
 - [26] N. Sarkar and P. Ghosh, Phys. Rev. **C 98**, 014907 (2018).
 - [27] P. Braun-Munzinger, K. Redlich and J. Stachel, nucl-th/0304013.
 - [28] A. Andronic, P. Braun-Munzinger and J. Stachel, Nucl. Phys. **A 772**, 167 (2006).
 - [29] D. H. Rischke, M. I. Gorenstein, H. Stoecker and W. Greiner, Z. Phys. **C 51**, 485 (1991).
 - [30] V. Vovchenko, D. V. Anchishkin, and M. I. Gorenstein, J. Phys. **A 48**, 305001 (2015).
 - [31] V. Vovchenko, D. V. Anchishkin, and M. I. Gorenstein, Phys. Rev. **C 91**, 064314 (2015).
 - [32] V. Vovchenko, D. V. Anchishkin, M. I. Gorenstein, and R. V. Poberezhnyuk, Phys. Rev. **C 92**, 054901 (2015).
 - [33] V. Vovchenko, M. I. Gorenstein, and H. Stoecker, Phys. Rev. Lett. **118**, 182301 (2017).
 - [34] Particle Data Group, J. Beringer et al., Phys. Rev. **D 86**, 010001 (2012).
 - [35] J. Cleymans and K. Redlich, Phys. Rev. Lett. **81**, 5284 (1998).
 - [36] J. Cleymans, H. Oeschler, K. Redlich, and S. Wheaton, Phys. Lett. **C 73**, 034905 (2006).
 - [37] K. Fukushima and Y. Hidaka, Phys. Rev. Lett. **117**, 102301 (2016).
 - [38] R. K. Mohapatra, arXiv:1711.06913 (Accepted by PRC)
 - [39] J. Cleymans, arXiv:1711.02882.